

DOCUMENT CONTROL SHEET

	ORIGINATOR'S REF. NLR-TP-2003-091		SECURITY CLASS. Unclassified
ORIGINATOR National Aerospace Laboratory NLR, Amsterdam, The Netherlands			
TITLE Modelling a spiralling type of non-locally reacting liner AIAA Paper 2003-3196			
PRESENTED AT The 9th AIAA/CEAS Aeroacoustics Conference as AIAA Paper 2003-3196, Hilton Head, South Carolina, USA, 12-14 May 2003			
AUTHORS P. Sijtsma and H.M. van der Wal	DATE March 2003	PP 13	REF 23
ABSTRACT In this paper, a non-locally reacting liner is considered, consisting of helical wave-guides filled with porous material, and covered with a perforated plate. This "spiralling" liner has more degrees of freedom than a conventional locally reacting liner. Apart from the cavity depth of the liner and the impedance of the perforated plate, also the properties of the porous material and the advance ratio of the helical wave-guides can be varied. The spiralling liner may be useful particularly for the reduction of rotor alone noise. The advance ratio of the wave-guides can then be tuned to the typical direction of noise propagation. The major part of this paper is about the mathematical modelling of the spiralling liner, with emphasis on the eigenvalue problem of a lined duct segment and the problem of matching with hard wall duct segments. Further, a validation experiment is described, by which good agreement was found with computed results. Finally, the results of a parametric study are summarised, showing the potential of this type of liner. For a typical case, 3 dB more reduction of rotor alone noise is predicted than with a locally-reacting liner.			



NLR-TP-2003-091

Modelling a spiralling type of non-locally reacting liner




AIAA Paper 2003-3196

P. Sijtsma and H.M. van der Wal

Presented as AIAA Paper 2003-3196 at the 9th AIAA/CEAS Aeroacoustics Conference, Hilton Head, South Carolina, USA, 12-14 May 2003

This report may be cited on condition that full credit is given to NLR and the authors.

Customer: National Aerospace Laboratory NLR
Working Plan number: A.1.C.2
Owner: National Aerospace Laboratory NLR
Division: Fluid Dynamics
Distribution: Unlimited
Classification title: Unclassified
March 2003

Approved by author:  27/03/03	Approved by project manager:  27/03/03	Approved by project managing department:  27/3/03
---	--	---



Contents

Nomenclature	3
I. Introduction	3
II. Theory	5
Equations in the duct	5
Equations in the liner	5
Boundary conditions	5
Eigenvalue equation	6
Solution of eigenvalue equation	7
Insertion Loss	7
Modal description	7
Mode matching at interfaces	8
Reflection at the inlet	9
Calculation of total acoustic field	9
III. Experimental validation	10
IV. Application	11
V. Conclusion	11
Acknowledgement	11
References	
2 Tables	
5 Figures	
Appendix: A method to solve the eigenvalue equation	12

(13 pages in total)



MODELLING A SPIRALLING TYPE OF NON-LOCALLY REACTING LINER

Pieter Sijtsma* and Henk M.M. van der Wal†

National Aerospace Laboratory NLR, 8300 AD Emmeloord, The Netherlands

In this paper, a non-locally reacting liner is considered, consisting of helical wave-guides filled with porous material, and covered with a perforated plate. This “spiralling” liner has more degrees of freedom than a conventional locally reacting liner. Apart from the cavity depth of the liner and the impedance of the perforated plate, also the properties of the porous material and the advance ratio of the helical wave-guides can be varied. The spiralling liner may be useful particularly for the reduction of rotor alone noise. The advance ratio of the wave-guides can then be tuned to the typical direction of noise propagation. The major part of this paper is about the mathematical modelling of the spiralling liner, with emphasis on the eigenvalue problem of a lined duct segment and the problem of matching with hard wall duct segments. Further, a validation experiment is described, by which good agreement was found with computed results. Finally, the results of a parametric study are summarised, showing the potential of this type of liner. For a typical case, 3 dB more reduction of rotor alone noise is predicted than with a locally-reacting liner.

Nomenclature

$A_{m\mu}$	= amplitude of right running mode
$B_{m\mu}$	= amplitude of left running mode
d	= liner thickness
f	= frequency (Hz)
i	= imaginary unit
J_m	= m^{th} order Bessel function of first kind
L	= axial co-ordinate of duct inlet, Fig. 2
M	= Mach number of duct flow
m	= circumferential mode number
p	= acoustic pressure in the duct
q	= acoustic pressure in the liner
S	= function describing helical fences, Eq. (6)
x_1, x_2	= axial co-ordinates of liner edge, Fig. 2
$U_{m\mu}$	= radial eigenfunction in hard wall duct segment
$V_{m\mu}$	= radial eigenfunction in lined duct segment
W_μ	= radial eigenfunction in the liner
Z_c	= characteristic impedance of porous material
Z_{total}	= total wall impedance, Eq. (13)
α	= axial wave number
$\alpha_{m\mu}$	= axial eigenvalue in lined duct segment
χ	= spiral angle
ε	= radial wave number in the duct, Eq. (19)
$\varepsilon_{m\mu}$	= radial eigenvalue in hard wall duct segment

$\kappa_{m\mu}$	= axial eigenvalue in hard wall duct segment
μ	= radial mode order
μ_{add}	= number of extra radial modes
μ_{max}	= number of radial modes
μ_p	= propagation constant of porous material
ω	= dimensionless frequency
ζ	= radial wave number in the liner, Eq. (28)

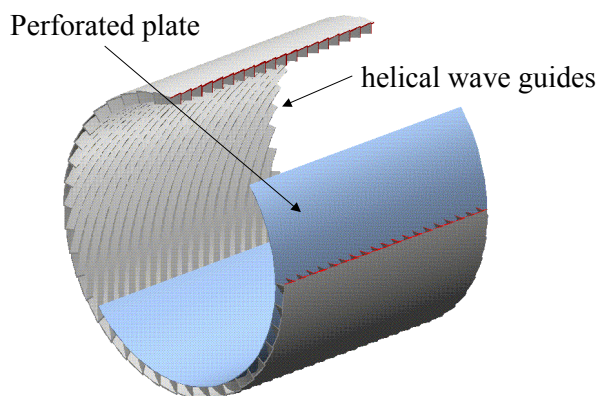


Fig. 1 “Spiralling” liner (drawn without porous material)

I. Introduction

In order to attenuate noise that is generated by an aircraft turbofan engine, usually locally reacting liners are applied. Such liners, which are applied at several positions in the wall of the engine flow duct, often consist of a single layer of honeycomb-arranged cavities, covered with a perforated plate, usually in

*Research Engineer, Aeroacoustics Department, P.O. Box 153, e-mail: sijtsma@nlr.nl.

†Research Engineer, Aeroacoustics Department, P.O. Box 153, e-mail: vdwal@nlr.nl.

Copyright © 2003 by the National Aerospace Laboratory NLR. Published by the American Institute of Aeronautics and Astronautics, Inc. with permission.



combination with a facing sheet. For specific flow conditions, there are essentially two degrees of freedom in the design of these locally reacting liners: the liner thickness (cavity depth) and the resistance of the perforated plate. If maximum attenuation is required of a sound field of single frequency and single circumferential mode, then these two degrees of freedom are sufficient to construct the optimum liner. Liner thickness and plate resistance can then be chosen such that the optimum effective wall impedance (ratio between acoustic wall pressure and acoustic velocity normal to the wall) is obtained.

If a sound field has to be attenuated that consists of several frequencies and/or modes, it may be interesting to consider liners with more degrees of freedom, for example locally reacting liners with multiple honeycomb layers. Alternatively, non-locally reacting liners may be considered, an example of which is discussed in this paper. This non-locally reacting liner consists of helical wave-guides, optionally filled with porous material and covered with a perforated plate (Fig. 1). This liner is called hereafter the “spiralling” liner. An extra degree of freedom compared to locally reacting liners, is the advance ratio of the wave-guides. Also the properties of the porous material can be varied. The effects of open helical wave-guides (without perforated plate and porous material) on sound attenuation have been studied before by Lohmann¹.

An interesting application for the spiralling liner could be the so-called fan-face liner. This is a liner of short length, just ahead of the main rotor of an aircraft engine, which is supposed to attenuate the ‘rotor alone noise’. This rotor alone noise, which consists of the blade-passing frequency and higher harmonics, propagates in a preferential direction. Therefore, it can be expected that the liner performance is sensitive to the advance ratio of the wave-guides, so that this extra degree of freedom may lead to more sound attenuation than the maximum reduction attainable with locally reacting liners.

The porous material is applied to avoid resonance inside the wave-guides. Moreover, with porous materials less thickness is required than with an empty liner, to realise the same characteristics. A disadvantage of the use of porous materials is the increase in weight. For a fan-face liner, of which the dimensions are moderate, this disadvantage might not be crucial.

The spiralling liner discussed here is related to the “bulk-absorbing liner” consisting of a layer of porous material, covered with a perforated plate. Bulk-absorbing liners or briefly “bulk-absorbers” have a

reputation to be less mode and frequency dependent than locally reacting liners^{2,3,4,5}.

The mathematical modelling of a liner consists of two parts. First, duct modes are constructed in a lined duct segment, by solving the appropriate eigenvalue problem. Then, these lined duct modes are matched with hard wall modes in other parts of the duct. Both parts of the modelling, each with its own difficulties, are discussed in this paper. A number of investigators^{5,6,7,8} has studied these issues for bulk-absorbers in circular ducts. The eigenvalue problem of spiralling liners has not been addressed before.

The duct modes for a spiralling liner are found by solving a coupled eigenvalue problem for the convective Helmholtz equation in the duct and an ordinary Helmholtz equation inside the helical wave-guides, that includes the effect of porous material. It is assumed that the wave-guides are so narrow that there is no sound propagation normal to the fences. Both Helmholtz equations are coupled through the impedance of the perforated plate. The duct mode problem boils down to an eigenvalue equation for the axial wave number, which can be solved numerically.

The porous material is assumed to be homogeneous and isotropic. Furthermore, it is assumed to be rigid, like glass fibre or metallic foam, so that the sound propagation is mainly through the pores and not through the material itself. As a result, we can describe the propagation of sound inside the porous material essentially by two complex quantities: the characteristic impedance and the propagation constant, both of which are frequency dependent^{5,4,9}.

The other part of the modelling is the matching of lined duct modes and hard wall modes. Basically, the matching is realised by prescribing continuity of pressure and axial velocity at the interface. In addition, the axial velocity inside the liner has to be set to zero at the edge. To set up (by Galerkin projection) a set of equations to solve this matching problem, the number of lined duct modes needs to be larger than the number of hard wall modes. The choice for the number of extra lined duct modes has to be done with caution.

Apart from the mathematical modelling, this paper also shows a comparison with Insertion Loss measurements with a spiralling liner barrel connected to a fan model in the NLR small anechoic wind tunnel KAT. Spinning modes were generated by a combination of rods and stator vanes. Finally, the results are shown of a typical liner optimisation study.



II. Theory

In this section all physical quantities have been made dimensionless using the ambient speed of sound, the ambient air density and the duct radius. A hub is not included in the present study. In the duct, cylindrical co-ordinates (x, r, θ) are defined. An acoustic field of single (non-dimensional) frequency ω will be considered and the factor $\exp(i\omega t)$ is suppressed throughout. The thickness of the perforated plate and the helical fences is neglected.

Equations in the duct

The acoustic pressure p in the duct ($r \leq 1$) is governed by the convective wave equation:

$$\nabla^2 p - \frac{D^2 p}{Dt^2} = 0, \quad (1)$$

where the ‘‘convective derivative’’ D/Dt is defined by

$$\frac{D}{Dt} = \frac{\partial}{\partial t} + M \frac{\partial}{\partial x} = i\omega + M \frac{\partial}{\partial x}, \quad (2)$$

in which M is the Mach number of the uniform steady axial flow. The acoustic velocity \mathbf{v} is related to the pressure via the momentum equation as follows:

$$\frac{D\mathbf{v}}{Dt} + \nabla p = i\omega\mathbf{v} + M \frac{\partial\mathbf{v}}{\partial x} + \nabla p = \mathbf{0}. \quad (3)$$

Equations in the liner

In the porous material inside the liner ($1 \leq r \leq 1+d$; d is the liner thickness), where there is no steady flow, the Helmholtz equation and the momentum equation for pressure q and velocity \mathbf{u} read^{3,4,9}

$$\nabla^2 q + \mu_p^2 q = 0, \quad (4)$$

$$i\mu_p Z_c \mathbf{u} + \nabla q = \mathbf{0}. \quad (5)$$

Herein, μ_p and Z_c are complex, frequency dependent numbers, describing the sound propagation through a porous material. The parameter μ_p is the so-called ‘‘propagation constant’’, and Z_c is the ‘‘characteristic impedance’’. This description assumes that the porous material is homogeneous, isotropic and rigid^{3,4,9}. If the liner is air-filled, we have $\mu_p = \omega$ and $Z_c = 1$.

An additional equation is needed to model the effect of the helical fences inside the liner. These fences are assumed to be aligned with helical planes:

$$S(x, \theta) = x \cos(\chi) + \theta \sin(\chi) = \text{Constant}. \quad (6)$$

The angle χ will be called ‘‘spiral angle’’. By this definition, the fences have r -independent pitch $2\pi \tan(\chi)$. It is assumed that the wave-guides are so narrow that there is no sound propagation normal to the fences, which yields the following condition for q :

$$\nabla q \cdot \nabla S = 0. \quad (7)$$

Summarised, in the spiralling liner the acoustic pressure q is governed by Eqs. (4) and (7).

Boundary conditions

The first boundary condition is the continuity of normal velocity across the perforated plate (at $r = 1$):

$$u_r = v_r^{\text{plate}}, \quad (8)$$

where v_r^{plate} is the normal velocity in the duct, but at a position attached to the perforated plate, where the steady flow speed is zero. To obtain an expression in terms of the pressure p , one can not directly apply (3) for the right-hand side of (8), because the normal velocity v_r is not continuous across the boundary layer. To obtain the correct expression, a precise analysis has to be carried out with a boundary layer of vanishing thickness^{10,11}.

The correct expression is obtained when continuity of ‘‘particle displacement’’, instead of the normal velocity, is prescribed across the boundary layer^{12,13}. The displacement vector \mathbf{D} is implicitly defined by

$$\mathbf{v} = \frac{D}{Dt} \mathbf{D} \text{ and } v_r^{\text{plate}} = \frac{\partial}{\partial t} D^{\text{plate}}. \quad (9)$$

Therefore, we have at $r = 1$

$$\frac{D u_r}{Dt} = \frac{D v_r^{\text{plate}}}{Dt} = \frac{\partial v_r}{\partial t}, \quad (10)$$

where $v_r|_{r=1}$ has to be interpreted as the limit of v_r for $r \uparrow 1$, not passing through the boundary layer.



The second boundary condition at $r=1$ is the relation between the pressure jump across the perforated plate and the normal velocity through it:

$$p - q = Z_0 u_r, \quad (11)$$

where Z_0 is the impedance of the plate. Using (3) and (10), the following expression is derived from (11):

$$\frac{D^2}{Dt^2} \left(\frac{p}{Z_{\text{total}}} \right) + \frac{\partial^2 p}{\partial t \partial r} = 0, \quad (12)$$

with

$$Z_{\text{total}} = Z_0 + \frac{q}{u_r} \Big|_{r=1}. \quad (13)$$

The ratio $q/u_r|_{r=1}$ is obtained by solving the governing equations inside the duct, including the hard wall boundary condition at the liner bottom $r = 1 + d$:

$$\frac{dq}{dr} = 0. \quad (14)$$

Assuming that Z_{total} is independent of x , we have:

$$-\frac{D^2 p}{Dt^2} \Big/ \frac{\partial^2 p}{\partial t \partial r} = Z_{\text{total}} \quad (15)$$

Eigenvalue equation

Consider a single mode:

$$p(x, r, \theta) = p(r) e^{i(\alpha x + m \theta)}. \quad (16)$$

From the convective wave equation (1), it follows that $p(r)$ has to satisfy the following differential equation:

$$\frac{d^2 p}{dr^2} + \frac{1}{r} \frac{dp}{dr} + \left((\omega + M\alpha)^2 - \alpha^2 - \frac{m^2}{r^2} \right) p = 0. \quad (17)$$

The solution of (17) reads (without hub)

$$p(r) = A J_m(\varepsilon r), \quad (18)$$

where A is a constant, J_m the m^{th} order Bessel functions of the first kind, and ε the radial wave number, given by the dispersion relation:

$$\varepsilon^2 = (\omega + M\alpha)^2 - \alpha^2. \quad (19)$$

The boundary condition (15) then turns into the eigenvalue equation:

$$\frac{(\omega + M\alpha)^2 J_m(\varepsilon)}{i\omega\varepsilon J'_m(\varepsilon)} = Z_{\text{total}}. \quad (20)$$

Mode shapes in lined sections are determined by the solutions of (20). For locally reacting liners, the right-hand side Z_{total} is independent of m and α . For the spiralling liner, an expression is derived below.

For a mode inside the liner, we write:

$$q(x, r, \theta) = q(r) \exp[iC(x \sin(\chi) - \theta \cos(\chi))], \quad (21)$$

by which condition (7) is satisfied. In the direction of the wave-guides, Eq. (6), the acoustic mode inside the liner must have the same periodicity as in the duct:

$$\left(\frac{\partial S}{\partial \theta} \frac{\partial q}{\partial x} - \frac{\partial S}{\partial x} \frac{\partial q}{\partial \theta} \right) / q = \left(\frac{\partial S}{\partial \theta} \frac{\partial p}{\partial x} - \frac{\partial S}{\partial x} \frac{\partial p}{\partial \theta} \right) / p, \quad (22)$$

which implies:

$$C = \alpha \sin(\chi) - m \cos(\chi) \quad (23)$$

and, hence,

$$q(x, r, \theta) = q(r) \exp[i(\alpha \sin(\chi) - m \cos(\chi)) \times (x \sin(\chi) - \theta \cos(\chi))]. \quad (24)$$

In order to solve equation (4), we approximate it as follows:

$$\begin{aligned} \nabla^2 q + \mu_p^2 q &= \frac{\partial^2 q}{\partial x^2} + \frac{1}{r} \frac{\partial}{\partial r} \left(r \frac{\partial q}{\partial r} \right) + \frac{\partial^2 q}{r^2 \partial \theta^2} + \mu_p^2 q \\ &\approx \frac{\partial^2 q}{\partial x^2} + \frac{\partial^2 q}{\partial r^2} + \frac{\partial^2 q}{\partial \theta^2} + \mu_p^2 q = 0. \end{aligned} \quad (25)$$

Substitution of (24) yields



$$\frac{d^2 q}{dr^2} + (\mu_p^2 - (\alpha \sin(\chi) - m \cos(\chi))^2) q = 0. \quad (26)$$

The general solution of (26), with boundary condition (14), is

$$q = B \cos(\zeta(r-1-d)), \quad (27)$$

with

$$\zeta^2 = \mu_p^2 - (\alpha \sin(\chi) - m \cos(\chi))^2. \quad (28)$$

For Z_{total} , (13), we have using (27) and (5)

$$Z_{\text{total}} = Z_0 - \frac{i\mu_p Z_c}{\zeta \tan(\zeta d)}. \quad (29)$$

Solution of eigenvalue equation

Eigenvalues α have to be solved from equation (20), with right-hand side (29). A possible method to determine these eigenvalues is to scan a relevant part of the complex plane. Each scan point serves as initial value for an iteration process (e.g. the Secant Method¹⁴), which leads to a solution of the eigenvalue equation. If the scan resolution is sufficiently high, all eigenvalues in the considered complex domain are found. This method is straightforward, but time-consuming, nevertheless feasible with the currently available computers. However, a smarter and much faster method is the application of solutions of limit cases as initial values¹⁵. This method is described in detail in the Appendix.

Insertion Loss

To evaluate the performance of a liner, the Insertion Loss (IL) is defined as the ratio between the acoustic power transmitted through the inlet plane ($x=L$ in Fig. 2) of the configurations with and without liner. It is usually expressed in dB:

$$\text{IL} = 10^{10} \log \left[\frac{\text{Power}(\text{unlined})}{\text{Power}(\text{lined})} \right]. \quad (30)$$

The acoustic power is defined as the integrated axial component of the acoustic intensity. The acoustic intensity is the time-averaged energy flux¹⁶.

Modal description

To calculate the acoustic power through the inlet plane from a given acoustic field at the source plane $x=0$, a modal description of the sound is used in the three regions of the duct (Fig. 2):

$$\begin{cases} \text{Region I} & : 0 \leq x \leq x_1, \\ \text{Region II} & : x_1 \leq x \leq x_2, \\ \text{Region III} & : x_2 \leq x \leq L. \end{cases} \quad (31)$$

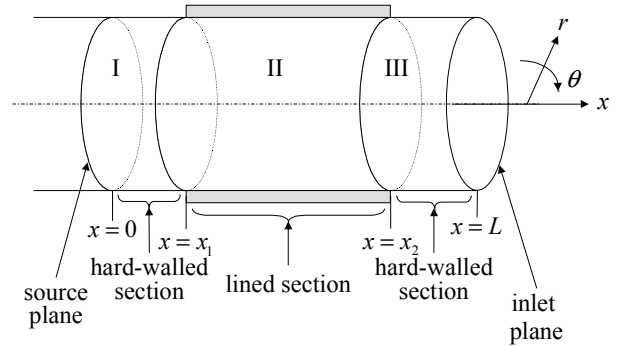


Fig. 2 Duct geometry

The modal description of the sound field in the different regions is as follows

$$p^{\text{I}}(x, r, \theta) = \sum_{m=-\infty}^{\infty} \sum_{\mu=1}^{\infty} \left\{ A_{m\mu}^{\text{I}} U_{m\mu}(r) e^{ik_{m\mu}^+ x} + B_{m\mu}^{\text{I}} U_{m\mu}(r) e^{ik_{m\mu}^- x} \right\} e^{im\theta}, \quad (32)$$

$$p^{\text{II}}(x, r, \theta) = \sum_{m=-\infty}^{\infty} \sum_{\mu=1}^{\infty} \left\{ A_{m\mu}^{\text{II}} V_{m\mu}^+(r) e^{i\alpha_{m\mu}^+ x} + B_{m\mu}^{\text{II}} V_{m\mu}^-(r) e^{i\alpha_{m\mu}^- x} \right\} e^{im\theta}, \quad (33)$$

$$p^{\text{III}}(x, r, \theta) = \sum_{m=-\infty}^{\infty} \sum_{\mu=1}^{\infty} \left\{ A_{m\mu}^{\text{III}} U_{m\mu}(r) e^{ik_{m\mu}^+ x} + B_{m\mu}^{\text{III}} U_{m\mu}(r) e^{ik_{m\mu}^- x} \right\} e^{im\theta}, \quad (34)$$

where $\kappa_{m\mu}^{\pm}$ and $\alpha_{m\mu}^{\pm}$ are solutions of the eigenvalue equation (20), with $Z_{\text{total}} = \infty$ (hard wall) for $\kappa_{m\mu}^{\pm}$ and Z_{total} given by (29) for $\alpha_{m\mu}^{\pm}$. The eigenfunctions $U_{m\mu}$ and $V_{m\mu}^{\pm}$ are normalised as

$$\int_0^1 r U_{m\mu}(r)^2 dr = \int_0^1 r |V_{m\mu}^{\pm}(r)|^2 dr = 1. \quad (35)$$

The superscripts “+” and “-” stand for “running in the positive x -direction” and “running in the negative x -direction”, respectively. The classification of



eigenvalues into “+” modes and “-” modes is done by the sign of the imaginary part of α (in case of real α , a small negative imaginary part is added to ω). This classification disregards the possible existence of unstable surface waves¹⁷. Herewith, numerical instabilities are avoided, possibly at the expense of physical reality.

We are interested in the acoustic power in region III. This is (still dimensionless)

$$\text{Power} = \frac{\pi\beta^4}{\omega} \sum_{m=-\infty}^{\infty} \sum_{\mu=1}^{\mu_0(m)} \beta_{m\mu} \times \left\{ \frac{|A_{m\mu}^{\text{III}}|^2}{(1-M\beta_{m\mu}/\omega)^2} - \frac{|B_{m\mu}^{\text{III}}|^2}{(1+M\beta_{m\mu}/\omega)^2} \right\}, \quad (36)$$

where $\mu_0(m)$ is the highest value of μ for which $\kappa_{m\mu}^{\pm}$ is real (in other words, $\mu_0(m)$ is the number of radial cut-on modes), and further

$$\beta^2 = 1 - M^2, \quad (37)$$

$$\beta_{m\mu} = \sqrt{\omega^2 - \beta^2 \varepsilon_{m\mu}^2}, \quad (38)$$

$$\begin{aligned} \varepsilon_{m\mu}^2 &= (\omega + M\kappa_{m\mu}^+)^2 - (\kappa_{m\mu}^+)^2 \\ &= (\omega + M\kappa_{m\mu}^-)^2 - (\kappa_{m\mu}^-)^2. \end{aligned} \quad (39)$$

Mode matching at interfaces

At the interfaces $x = x_1$ and $x = x_2$ (Fig. 2) continuity of pressure p and axial velocity v_x is prescribed. Furthermore, we prescribe at the liner termination $1 \leq r \leq 1+d$ the axial velocity u_x to vanish. At the interface $x = x_1$ and for fixed m , this is worked out below.

The interface conditions are:

$$p^1(x_1, r, \theta) = p^{\text{II}}(x_1, r, \theta), \quad 0 \leq r \leq 1, \quad (40)$$

$$v_x^1(x_1, r, \theta) = v_x^{\text{II}}(x_1, r, \theta), \quad 0 \leq r \leq 1, \quad (41)$$

$$u_x^{\text{II}}(x_1, r, \theta) = 0, \quad 1 \leq r \leq 1+d, \quad (42)$$

The acoustic pressure is written as a finite number of acoustic modes (cf. Eqs. (32) and (33)):

$$p^1(x, r, \theta) = \sum_{\mu=1}^{\mu_{\text{max}}} \left\{ A_{m\mu}^1 U_{m\mu}(r) e^{i\kappa_{m\mu}^+ x} + B_{m\mu}^1 U_{m\mu}(r) e^{i\kappa_{m\mu}^- x} \right\} e^{im\theta}, \quad (43)$$

$$p^{\text{II}}(x, r, \theta) = \sum_{\mu=1}^{\mu_{\text{max}} + \mu_{\text{add}}} \left\{ A_{m\mu}^{\text{II}} V_{m\mu}^+(r) e^{i\kappa_{m\mu}^+ x} + B_{m\mu}^{\text{II}} V_{m\mu}^-(r) e^{i\kappa_{m\mu}^- x} \right\} e^{im\theta}, \quad (44)$$

In the lined section (II), the number of unknowns is increased by μ_{add} , in order to have additional degrees of freedom to satisfy the hard wall condition (42) at the liner termination. The unknown coefficients $A_{m\mu}^{\text{II}}$ and $B_{m\mu}^{\text{II}}$ are solved by applying Galerkin projection to Eqs. (40)-(42):

$$\int_0^1 r U_{m\mu}(r) p^1(x_1, r, \theta) dr = \int_0^1 r U_{m\mu}(r) p^{\text{II}}(x_1, r, \theta) dr, \quad \mu = 1, \dots, \mu_{\text{max}}, \quad (45)$$

$$\int_0^1 r U_{m\mu}(r) v_x^1(x_1, r, \theta) dr = \int_0^1 r U_{m\mu}(r) v_x^{\text{II}}(x_1, r, \theta) dr, \quad \mu = 1, \dots, \mu_{\text{max}}, \quad (46)$$

$$\int_1^{1+d} W_{\mu}(r) u_x^{\text{II}}(x_1, r, \theta) dr = 0, \quad \mu = 1, \dots, \mu_{\text{add}}, \quad (47)$$

where W_{μ} are “hard-wall eigensolutions” inside the liner, i.e., functions satisfying

$$\frac{d^2 W_{\mu}}{dr^2} + \eta^2 W_{\mu} = 0 \quad (48)$$

and

$$W_{\mu}'(1) = W_{\mu}'(1+d) = 0. \quad (49)$$

In total, we have $2\mu_{\text{max}} + \mu_{\text{add}}$ unknowns in Eqs. (43) and (44), and the same number of equations (45)-(47).

The choice for the number μ_{add} must be done with caution. We choose μ_{add} such that the imaginary part of the highest hard wall eigenvalue inside the liner just does not exceed the imaginary part of the highest hard wall eigenvalue inside the duct. Then, it is expected that the so-called edge condition (the internal energy of the field in the neighbourhood of an edge has to be finite¹⁸) is fulfilled.

Substitution of (43) and (44) into (45), (46) and (47) yields



$$\sum_{\nu=1}^{\mu_{\max}} \left\{ a_{\mu\nu}^+ A_{m\nu}^I e^{ik_{m\nu}^+ x_1} + a_{\mu\nu}^- B_{m\nu}^I e^{ik_{m\nu}^- x_1} \right\} = \sum_{\nu=1}^{\mu_{\max} + \mu_{\text{add}}} \left\{ c_{\mu\nu}^+ A_{m\nu}^{II} e^{i\alpha_{m\nu}^+ x_1} + c_{\mu\nu}^- B_{m\nu}^{II} e^{i\alpha_{m\nu}^- x_1} \right\}, \quad (50)$$

$$\mu = 1, \dots, \mu_{\max},$$

$$\sum_{\nu=1}^{\mu_{\max}} \left\{ b_{\mu\nu}^+ A_{m\nu}^I e^{ik_{m\nu}^+ x_1} + b_{\mu\nu}^- B_{m\nu}^I e^{ik_{m\nu}^- x_1} \right\} = \sum_{\nu=1}^{\mu_{\max} + \mu_{\text{add}}} \left\{ d_{\mu\nu}^+ A_{m\nu}^{II} e^{i\alpha_{m\nu}^+ x_1} + d_{\mu\nu}^- B_{m\nu}^{II} e^{i\alpha_{m\nu}^- x_1} \right\}, \quad (51)$$

$$\mu = 1, \dots, \mu_{\max},$$

$$\sum_{\nu=1}^{\mu_{\max} + \mu_{\text{add}}} \left\{ f_{\mu\nu}^+ A_{m\nu}^{II} e^{i\alpha_{m\nu}^+ x_1} + f_{\mu\nu}^- B_{m\nu}^{II} e^{i\alpha_{m\nu}^- x_1} \right\} = 0, \quad (52)$$

$$\mu = 1, \dots, \mu_{\text{add}}.$$

Using some results from the theory of Bessel functions¹⁹, and omitting some constants, the following expressions for the coefficients $a_{\mu\nu}^{\pm}$, $b_{\mu\nu}^{\pm}$, $c_{\mu\nu}^{\pm}$, $d_{\mu\nu}^{\pm}$ and $f_{\mu\nu}^{\pm}$ can be derived:

$$a_{\mu\nu}^{\pm} = \delta_{\mu\nu}, \quad (53)$$

$$b_{\mu\nu}^{\pm} = \delta_{\mu\nu} \frac{k_{m\nu}^{\pm}}{\omega + Mk_{m\nu}^{\pm}}, \quad (54)$$

$$c_{\mu\nu}^{\pm} = \frac{1}{\varepsilon_{m\mu}^2 - (\omega + M\alpha_{m\nu}^{\pm})^2 + (\alpha_{m\nu}^{\pm})^2} \times U_{m\mu}(1) V_{m\nu}^{\pm \prime}(1), \quad (55)$$

$$d_{\mu\nu}^{\pm} = \frac{1}{\varepsilon_{m\mu}^2 - (\omega + M\alpha_{m\nu}^{\pm})^2 + (\alpha_{m\nu}^{\pm})^2} \times U_{m\mu}(1) V_{m\nu}^{\pm \prime}(1) \frac{\alpha_{m\nu}^{\pm}}{\omega + M\alpha_{m\nu}^{\pm}}, \quad (56)$$

$$f_{\mu\nu}^{\pm} = \frac{1}{\eta_{\mu}^2 - \mu^2 + (\alpha_{m\nu}^{\pm} \sin(\chi) - m \cos(\chi))^2} \times V_{m\nu}^{\pm \prime}(1) \frac{\alpha_{m\nu}^{\pm}}{(\omega + M\alpha_{m\nu}^{\pm})^2}. \quad (57)$$

In (53) en (54), $\delta_{\mu\nu}$ is the ‘‘Kronecker delta’’:

$$\delta_{\mu\nu} = \begin{cases} 1, & \text{for } \mu = \nu, \\ 0, & \text{for } \mu \neq \nu. \end{cases} \quad (58)$$

In (57), η_{μ} are radial eigenvalues of (48) with (49):

$$\eta_{\mu} = (\mu - 1)\pi/d. \quad (59)$$

We can write the system (50)-(52) in matrix notation as:

$$\begin{cases} \mathbf{a}^+ \mathbf{A}^I + \mathbf{a}^- \mathbf{B}^I = \mathbf{c}^+ \mathbf{A}^{II} + \mathbf{c}^- \mathbf{B}^{II}, \\ \mathbf{b}^+ \mathbf{A}^I + \mathbf{b}^- \mathbf{B}^I = \mathbf{d}^+ \mathbf{A}^{II} + \mathbf{d}^- \mathbf{B}^{II}, \\ \mathbf{f}^+ \mathbf{A}^{II} + \mathbf{f}^- \mathbf{B}^{II} = \mathbf{0}. \end{cases} \quad (60)$$

Reorganising the system (60) such that the unknown vectors \mathbf{A}^{II} and \mathbf{B}^I are in the left-hand side and the known vectors \mathbf{A}^I and \mathbf{B}^{II} are in the right-hand side, leads to the following matrix equation:

$$\begin{pmatrix} \mathbf{c}^+ & -\mathbf{a}^- \\ \mathbf{d}^+ & -\mathbf{b}^- \\ \mathbf{f}^+ & \mathbf{0} \end{pmatrix} \begin{pmatrix} \mathbf{A}^{II} \\ \mathbf{B}^I \end{pmatrix} = \begin{pmatrix} \mathbf{a}^+ & -\mathbf{c}^- \\ \mathbf{b}^+ & -\mathbf{d}^- \\ \mathbf{0} & -\mathbf{f}^- \end{pmatrix} \begin{pmatrix} \mathbf{A}^I \\ \mathbf{B}^{II} \end{pmatrix}. \quad (61)$$

For high frequencies, the system can become ill-conditioned. Then it may be necessary to use a matrix regularisation technique¹⁴ to obtain solutions.

Reflection at the inlet

At the inlet $x = L$ (Fig. 2) acoustic modes are reflected. The reflection matrix, by which $B_{m\mu}^{III}$, $\mu = 1, \dots, \mu_{\max}$ can be calculated from $A_{m\mu}^{III}$, $\mu = 1, \dots, \mu_{\max}$ can, for instance, be obtained from a Wiener-Hopf technique, assuming an unflanged open duct end²⁰.

Calculation of total acoustic field

The total induced acoustic field in the duct, i.e., all unknown amplitudes $A_{m\mu}^{II}$, $A_{m\mu}^{III}$, $B_{m\mu}^I$, $B_{m\mu}^{II}$, $B_{m\mu}^{III}$ are calculated from the input amplitudes $A_{m\mu}^I$ by an iterative procedure, as follows¹⁰.

- (0) Set $A_{m\mu}^{II} = A_{m\mu}^{III} = B_{m\mu}^I = B_{m\mu}^{II} = B_{m\mu}^{III} = 0$, for all μ .
- (1) Calculate $A_{m\mu}^{II}$ and $B_{m\mu}^I$ from $A_{m\mu}^I$ and $B_{m\mu}^{II}$ by the matching equations at $x = x_1$.
- (2) Calculate $A_{m\mu}^{III}$ and $B_{m\mu}^{II}$ from $A_{m\mu}^{II}$ and $B_{m\mu}^{III}$ by the matching equations at $x = x_2$.
- (3) Calculate $B_{m\mu}^{III}$ from $A_{m\mu}^{III}$ by the reflection matrix at $x = L$ (optional).
- (4) In case of insufficient convergence, go to step 1.



III. Experimental validation

Within the EU project “RANNTAC”, an experiment was carried out with an air-filled spiralling liner, in the NLR small anechoic wind tunnel KAT. As a reference, also a locally reacting liner was tested. A few relevant characteristics are given below.

The duct diameter as well as the liner length was 400 mm. The liner cavity depths were 25 mm for the locally reacting liner and 18 mm for the spiralling liner. The width of the helical wave-guides was also 18 mm. The liner barrel was connected to a fan model (Fig. 3). The sound field was generated by a rotor-stator combination consisting of a rotor with 16 rods and a stator with 9 vanes. The rotation speed was 6850 RPM. The Mach number in the duct was $M = -0.16$.



Fig. 3 Liner barrel connected to fan model in NLR's anechoic wind tunnel KAT

Acoustic modes were generated at multiples of the blade passing frequency: $f = n \times 16 \times 6850 / 60$, with circumferential mode numbers $m = 16n - 9k$. Note that, in contrast with Eq. (16), the $\exp(-im\theta)$ convention is used here. For validation of the theory, measured results were used up to the 4th harmonic ($n = 4$). The cut-on modes for these harmonics are listed in Table 1.

Table 1 Cut-on modes in validation experiment

n	f	m
1	1826.67	-2
2	3653.33	-4, 5
3	5480.00	-15, -6, 3, 12
4	7306.67	-17, -8, 1, 10, 19

The helical wave-guides of the spiralling liner had the same direction as the rotor relative air speed. The spiral angle, Eq. (6), was $\chi = 32.5^\circ$.

The impedance of the perforated plate that covered the spiralling liner was obtained experimentally on an instrumented locally reacting liner sample. The locally reacting liner was covered with a so-called “Screen On Perforate”, of which the impedance is the sum of a frequency-independent specific acoustic resistance and a frequency-dependent mass-reactance²¹. The plate impedances used are listed in Table 2.

Table 2 Plate impedances (non-dimensional) in validation experiment

n	Locally reacting	Spiralling liner
1	(1.460, 0.337)	(0.565, 0.260)
2	(1.460, 0.675)	(0.627, 0.525)
3	(1.460, 1.012)	(0.690, 0.790)
4	(1.460, 1.349)	(0.753, 1.054)

The tests were set up for validation purposes only. No conclusions can be drawn about the appropriateness of the different liners. For cost efficiency, the spiralling liner was not filled with porous material. When the wave-guides are filled with a porous material, a much better performance is expected.

For the two types of liners and for the input modes mentioned in Table 1, measured and calculated Insertion Loss were compared. The results are plotted in Fig. 4 (locally reacting liner) and Fig. 5 (spiralling liner). In general, the agreement is good.

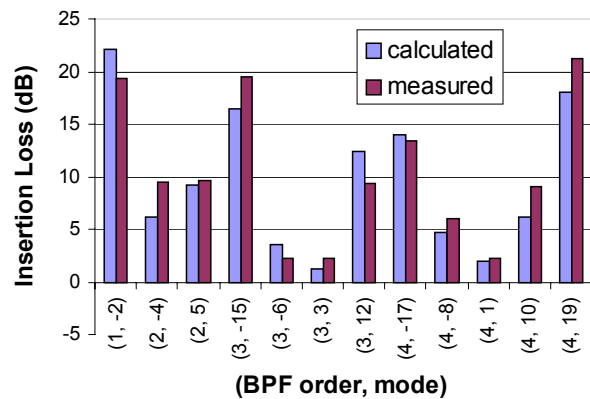


Fig. 4 Comparison of calculated and measured Insertion Loss: locally reacting liner

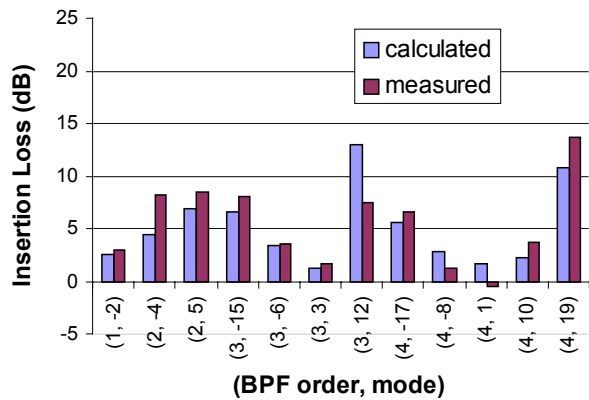


Fig. 5 Comparison of calculated and measured Insertion Loss: spiralling liner

IV. Application

This section contains a summary of a parametric study carried out in the RANNTAC project. Herein, we had for the length and the thickness of the liner (relative to the duct radius):

$$x_2 - x_1 = 1.0, \quad (62)$$

$$d = 0.06. \quad (63)$$

For the porous material inside the spiralling liner, approximate properties of the metal foam “Retimet” were used, which were measured in an impedance tube at NLR, using the transfer function method of Utsuno et al.²². The used values are:

$$\frac{\mu_p}{\omega} = Z_c = \left(1.6 - \frac{36}{\omega} i\right)^{1/2}. \quad (64)$$

For locally reacting and spiralling liners, an optimisation study was performed for “broadband” input at the source plane (all cut-on modes of a wide range of frequencies are present with equal energy per mode). Because of the symmetric input, the optimum spiral angle was $\chi = 0$ (ring-shaped wave-guides). The difference in performance between both types of liner for broadband noise appeared to be negligible.

However, it was found that the spiralling liner performed 2 dB better for a typical “rotor alone noise” spectrum at Sideline conditions. The Insertion Loss using the locally-reaction liner was 18.7 dB. Using the spiralling liner, it was 20.8 dB. By varying the spiral angle χ , the Insertion Loss could be enlarged to 21.7 dB, which is 3 dB better than the locally reacting

liner. The optimum spiral angle was found at $\chi = 53^\circ$.

For broadband noise, this spiralling liner with $\chi = 53^\circ$ performed almost the same as the spiralling liner with $\chi = 0$, and, hence, almost the same as the locally reacting liner.

V. Conclusion

A theoretical model was described of a spiralling type of non-locally reacting liner, consisting of helical wave-guides filled with porous material, covered by a perforated plate. The theory was validated experimentally. The agreement between theory and experimental results was good. A liner optimisation study, with broadband noise input, showed negligible difference in performance between the optimum locally reacting liner and the optimum spiralling liner. However, for a typical rotor alone noise input, 3 dB more reduction was found with the spiralling liner. This was achieved by optimising the advance ratio of the wave-guides.

Acknowledgement

This study was carried out within the research project RANNTAC (Reduction of Aircraft Noise by Nacelle Treatment and Active Control), which was sponsored by the European Union.

References

- ¹Lohmann, D., “Acoustic wave propagation in cylindrical ducts with helical inserts” (in German), DFVLR Forschungsbericht 78-30, 1978.
- ²Ingard, K.U., “Locally and non-locally reacting flexible porous layers; a comparison of acoustical properties”, Transactions of the ASME, Vol. 103, pp. 302-313, 1981.
- ³Morse, P.M., and Ingard, K.U., *Theoretical Acoustics*, McGraw-Hill, 1968.
- ⁴Nayfeh, A.H., Kaiser, J.E., and Telionis, D.P., “Acoustics of aircraft engine-duct systems”, *AIAA Journal*, Vol. 13, No. 2, pp. 130-153, 1975.
- ⁵Sun, J., “Effects of isotropic and anisotropic bulk liners on wave propagation in duct carrying flows”, PhD thesis, Virginia Polytechnic Institute and State University, 1975.
- ⁶Nilsson, B.E., “The propagation of sound in cylindrical ducts with mean flow and bulk-reacting lining”, PhD thesis, University of Gothenburg, Sweden, 1980.
- ⁷Cummings, A., and Chang, I.-J., “Sound attenuation of a finite length dissipative flow duct silencer with internal mean flow in the absorbent”, *Journal of Sound and Vibration*, Vol. 127, No. 1, pp. 1-17, 1988.



⁸Bies, D.A., Hansen, C.H., and Bridges, G.E., "Sound attenuation in rectangular and circular cross section ducts with flow and bulk-reacting liner", *Journal of Sound and Vibration*, Vol. 146, No. 1, pp. 47-80, 1991.

⁹Bies, D.A., "Acoustic properties of porous materials", in *Noise and Vibration Control*, edited by L.L. Beranek, McGraw-Hill, pp. 245-269, 1971.

¹⁰Rienstra, S.W., "The acoustics of a lined duct with flow", NLR Technical Report 87002, 1987.

¹¹Eversman, W., "Approximation for thin boundary layers in the sheared flow duct transmission problem", *Journal of the Acoustical Society of America*, Vol. 53, No. 5, pp. 1346-1350, 1973.

¹²Miles, J.W., "On the reflection of sound at an interface of relative motion", *Journal of the Acoustical Society of America*, Vol. 29, No. 2, pp. 226-228, 1957.

¹³Ribner, H.S., "Reflection, transmission and amplification of sound by a moving medium", *Journal of the Acoustical Society of America*, Vol. 29, No. 4, pp. 435-441, 1957.

¹⁴Press, W.H., Teukolski, S.A., Vetterling, W.T. and Flannery, B.P., *Numerical Recipes*, Cambridge, 1994.

¹⁵Eversman, W., "Initial values for the integration scheme to compute the eigenvalues for propagation in ducts", *Journal of Sound and Vibration*, Vol. 50, No. 1, pp. 159-162, 1977.

¹⁶Goldstein, M.E., *Aeroacoustics*, McGraw-Hill, 1976

¹⁷Rienstra, S.W., "Hydrodynamic instabilities and surface waves in a flow over an impedance wall", in: *Aero- and Hydro-Acoustics*, IUTAM Symposium Lyon, Eds. G. Comte-Bellot and J.E. Ffowcs Williams, Springer, pp. 483-490, 1986 also NLR MP 85053.

¹⁸Mitra, R., and Lee, S.W., *Analytical techniques in theory of guided waves*, McMillan, 1971.

¹⁹Watson, G.N., *A treatise on the theory of Bessel functions*, Cambridge, 1966.

²⁰Rienstra, S.W., "Acoustic radiation from a semi-infinite annular duct in a uniform subsonic main flow", *Journal of Sound and Vibration*, Vol. 94, No. 2, pp. 267-288, 1984 also NLR MP 82045.

²¹Guess, A.W., "Calculation of perforated plate liner parameters from specified acoustic resistance and reactance", *Journal of Sound and Vibration*, Vol. 40, No. 1, pp. 119-137, 1975.

²²Utsuno, H., Toshimitsu, T. and Fujikawa, T., "Transfer function method for measuring characteristic impedance and propagation constant of porous materials", *Journal of the Acoustical Society of America*, Vol. 86, No. 2, pp. 637-643, 1989.

²³Tester, B.J., "The propagation and attenuation of sound in lined ducts containing uniform or 'plug' flow", *Journal of Sound and Vibration*, Vol. 28, No. 2, pp. 151-203, 1973.

Appendix: A method to solve the eigenvalue equation

Restatement of the problem

The eigenvalue equation (20), with (29) is rewritten here as:

$$V(\alpha) + W(\alpha) - Z_0 = 0, \quad (65)$$

with

$$V(\alpha) = \frac{(\omega + M\alpha)^2 J_m(\varepsilon)}{i\omega\varepsilon J'_m(\varepsilon)} \quad (66)$$

and

$$W(\alpha) = \frac{i\mu_p Z_c}{\zeta \tan(\zeta d)}. \quad (67)$$

Initial values

As initial values for iterations leading to solutions of (65), we use poles and zeros of V and W , i.e., solutions of $V(\alpha) = \infty$, $V(\alpha) = 0$, $W(\alpha) = \infty$ and $W(\alpha) = 0$. Zeros and poles of V can be found by solving, respectively,

$$J'_m(\varepsilon) = 0 \quad (68)$$

and

$$J_m(\varepsilon) = 0. \quad (69)$$

Both (68) and (69) only have real solutions¹⁹. Poles and zeros of W are, respectively,

$$\alpha = \frac{m \cos(\chi) \pm \sqrt{\mu_p^2 - ((j-1)\pi/d)^2}}{\sin(\chi)}, \quad j = 1, 2, \dots \quad (70)$$

and

$$\alpha = \frac{m \cos(\chi) \pm \sqrt{\mu_p^2 - ((j-\frac{1}{2})\pi/d)^2}}{\sin(\chi)}, \quad j = 1, 2, \dots \quad (71)$$

Special initial values: surface waves

To be certain that the special surface waves^{17,23} are included, also the solutions of the "surface wave equation" are used as initial values. The surface wave equation is the asymptotic expression of (65) which



remains for large positive real values of γ_1 and γ_2 , after insertion of $p(r) = e^{-\gamma_1(1-r)}$ and $q(r) = e^{-\gamma_2(r-1)}$ into the governing equations for p and q . It can be shown that the following asymptotic expressions remain:

$$V(\alpha) \rightarrow -\frac{i(\omega + M\alpha)^2}{\omega\gamma_1}, \quad \gamma_1^2 = -\varepsilon^2, \quad (72)$$

$$W(\alpha) \rightarrow -\frac{i\mu_p Z_c}{\gamma_2}, \quad \gamma_2^2 = -\zeta^2, \quad (73)$$

where ε is given by (19) and ζ by (28). It follows that the surface wave equation becomes

$$-\frac{i(\omega + M\alpha)^2}{\omega\gamma_1} - \frac{i\mu_p Z_c}{\gamma_2} - Z_0 = 0, \quad (74)$$

which implies

$$4\omega^2 \gamma_1^2 \gamma_2^2 (\omega + M\alpha)^4 \mu_p^2 Z_c^2 - \left(\omega^2 \gamma_1^2 \gamma_2^2 Z_0^2 + \gamma_2^2 (\omega + M\alpha)^4 + \omega^2 \gamma_1^2 \mu_p^2 Z_c^2 \right)^2 = 0. \quad (75)$$

This is a 12th order polynomial in α , which can be solved by a standard technique.

Iteration

A number of equivalent formulations of the eigenvalue equation (65) is used, all of which have the same solutions

$$F_1(\alpha) = V(\alpha) + W(\alpha) - Z_0, \quad (76)$$

$$F_2(\alpha) = \frac{1}{V(\alpha)} + \frac{1}{W(\alpha) - Z_0}, \quad (77)$$

$$F_3(\alpha) = \frac{1}{V(\alpha) - Z_0} + \frac{1}{W(\alpha)}, \quad (78)$$

$$F_4(\alpha) = (\alpha - \alpha_{\text{ref}})(V(\alpha) + W(\alpha) - Z_0), \quad (79)$$

with $V(\alpha_{\text{ref}}) = \infty$ or $W(\alpha_{\text{ref}}) = \infty$,

$$F_5(\alpha) = (\alpha - \alpha_{\text{ref}}) \left(\frac{1}{V(\alpha)} + \frac{1}{W(\alpha) - Z_0} \right), \quad (80)$$

with $V(\alpha_{\text{ref}}) = 0$,

$$F_6(\alpha) = (\alpha - \alpha_{\text{ref}}) \left(\frac{1}{V(\alpha) - Z_0} + \frac{1}{W(\alpha)} \right), \quad (81)$$

with $W(\alpha_{\text{ref}}) = 0$.

The search process can be done with the Newton-Raphson Method¹⁴:

$$\alpha_{n+1} = \alpha_n - \frac{F_j(\alpha_n)}{F_j'(\alpha_n)} \quad (82)$$

or with the Secant Method¹⁴:

$$\alpha_{n+1} = \alpha_n - \frac{F_j(\alpha_n)(\alpha_n - \alpha_{n-1})}{F_j(\alpha_n) - F_j(\alpha_{n-1})}. \quad (83)$$

In the procedure followed here, the first step in the iteration process is done with Newton Raphson, the others with the Secant Method. When surface waves are used as initial values, all steps are done with the Secant Method. The functions F_j are used according to the scheme below.

<u>Initial values</u>	<u>First step</u>	<u>Other steps</u>
Zeros of V	F_1	F_5
First pole of V	F_2	F_1
Other poles of V	F_2	F_4
Zeros of W	F_1	F_6
Poles of W	F_3	F_4
Surface waves	F_4	F_4

For α_{ref} in F_4 , F_5 and F_6 the initial value are used, except for the case of the surface waves. Then, a lowest order pole of V or W is used, whichever is the closest to the initial value.